

A condensed phase decomposition mechanism for ammonium nitrate

Yu-ichiro Izato* and Atsumi Miyake*†

*Graduate School of Environment and Information Science, Yokohama National University

79-7 Tokiwadai, Hodogaya-ku, Yokohama 240-8501, JAPAN

Phone : +45-339-3993

†Corresponding author : atsumi@ynu.ac.jp

Received : November 17, 2014 Accepted : April 13, 2015

Abstract

The purpose of this study was to develop an improved understanding of the condensed phase decomposition mechanism of ammonium nitrate (AN). To this end, the thermal properties of AN were studied using pressurized differential scanning calorimetry (PDSC), and evolved gases were analyzed by combining PDSC with Fourier transform infrared spectroscopy (PDSC-FTIR) and mass spectrometry (PDSC-MS). PDSC results showed that AN undergoes an exothermic reaction above 0.3 MPa, and that this exothermic reaction offsets the endothermic reaction of AN as the ambient pressure is increased. Evolved gas analyses demonstrated that AN generates N_2O and H_2O during the exotherm and NO_2 throughout the endotherm. The heat flow associated with the thermal decomposition of AN was simulated assuming that the decomposition rate of AN is given by $-dC_{AN}/dt = 10^{9.4} \exp(-126000/RT) C_{NH_4^+} C_{HNO_3}$, that the heat of reaction is 105 kJ as per the reaction equation $HNO_3(l) + NH_4^+(l) = N_2O(g) + H_3O^+(l) + H_2O(g) + 105 kJ$ and that $C_{NH_4^+}$ and C_{HNO_3} are constant due to chemical equilibrium. The heat flow curves calculated in this manner are in good agreement with the experimental DSC curves obtained at 1.1 MPa.

Keywords : ammonium nitrate, thermal decomposition, condensed phase decomposition, thermal analysis, evolved gas analysis

1. Introduction

Ammonium nitrate (AN) is widely used as a fertilizer and as an ingredient in industrial explosives and oxidizing chemical compositions because it is relatively cheap, releases almost 100% gaseous products upon reaction, and has a positive oxygen balance (+20.0 g g^{-1}). In addition, combinations of AN with suitable combustibles have been proposed as gas-forming agents for automotive air-bag deployment systems and as next-generation halogen-free propellants¹⁾.

Unfortunately, tragic accidental explosions involving AN have occurred in the past^{2)–5)}, including incidents at a West Fertilizer Company storage facility in Texas in 2013⁴⁾ and at an AZF plant in Toulouse, France in 2001⁵⁾.

To allow the safe development and use of AN-containing devices, it is important to understand the reaction mechanisms, combustion performances and thermal stabilities of AN compositions. As such, there have been

many studies on the decomposition and combustion mechanisms of AN compositions^{2), 6)–35)}.

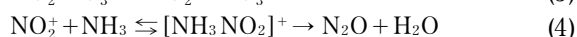
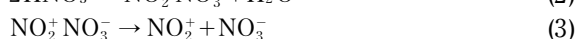
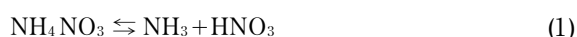
The combustion of energetic materials, including AN, is typically characterized by a diverse range of physical and chemical processes that occur in a complex series of stages, and analyzing the behavior of an energetic material in the condensed phase is therefore an important step in obtaining a better understanding of its combustion behavior. Sinditskii et al. studied the decomposition and combustion of condensed phase AN at the burning surface and showed that heat release from the condensed phase affected the combustion characteristics. They subsequently proposed various condensed phase combustion models^{6), 7)}. The present authors have studied the thermal decomposition and combustion mechanisms of AN/carbon mixtures^{8)–12)}, and determined that sustainable combustion is associated with exothermic decomposition of the condensed phase⁹⁾.

The aim of the present study was to gain a better understanding of condensed phase decomposition (CPD) in molten AN. As such, we analyzed the thermal behavior of AN under high pressure and also studied the evolved gases. The experimental results were compared with the theoretically predicted thermal behavior of AN based on chemical equilibrium calculations.

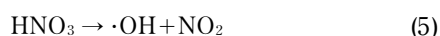
2. Thermal decomposition mechanism of ammonium nitrate

Oxley reported that the decomposition mechanism of AN involves two pathways: an ionic reaction and a radical reaction. The ionic reaction occurs at low temperatures and proceeds relatively slowly while the radical reaction involves active radicals and takes place at high temperatures at high speed^{2, 13}.

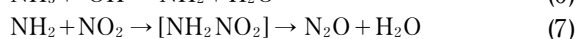
AN melts at 169 °C and begins to decompose as soon as it melts. The first step of the ionic reaction involves the dissociation of NH_4NO_3 into NH_3 and HNO_3 , followed by the oxidation of NH_3 by HNO_3 as shown in the following Equations (1)-(4)^{2, 13}.



As the temperature increases, the ionic decomposition of AN is overtaken by radical reactions. Brower determined the mechanism for the radical reaction of AN in the high temperature state above 300 °C. In this mechanism, AN initially dissociates into HNO_3 and NH_3 -like ions [Equation (1)] while the subsequent step is the homolysis of the O-N bond in HNO_3 , as shown in Equation (5)¹⁴.



Following this homolysis, a high-speed radical chain reaction develops, as summarized by Equations (6) - (7). However, since the activation energy for the homolysis of HNO_3 is very high, at approximately 190 kJ mol^{-1} , this represents the rate-controlling step¹⁴.



Manelis et al. determined that the rate of thermal decomposition of AN may be expressed by Equation (8)¹⁵.

$$-dC_{\text{AN}}/dt = 2k_1C_{\text{N}_2\text{O}_5} + k_2C_{\text{NH}_4^+}C_{\text{N}_2\text{O}_5} + k_3C_{\text{NH}_4^+}C_{\text{HNO}_3} \quad (8)$$

Here C_i is the concentration of chemical species i [mol L^{-1}], t is time [s], and k is the rate constant. The decomposition typically proceeds primarily through the oxidation of NH_4^+ by HNO_3 , and so the main contribution is from the third term of Equation (8), although in systems with a large excess of HNO_3 the predominant reaction mechanism transitions to oxidation by N_2O_5 ¹⁵. The thermal decomposition rate for AN under typical conditions can therefore be described as in Equations (9) and (10).

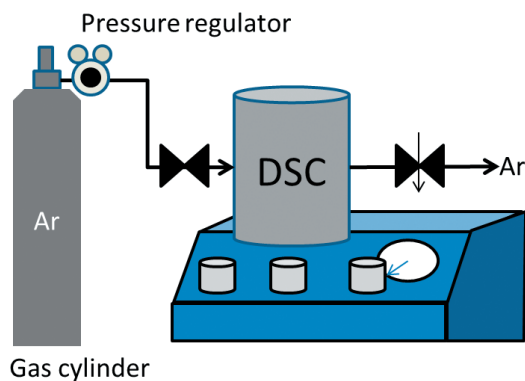


Figure 1 Experimental setup of PDSC.

$$-dC_{\text{AN}}/dt \cong k_3C_{\text{NH}_4^+}C_{\text{HNO}_3} \quad (9)$$

$$k_3 = 10^{9.4} \exp(-125520/RT), \text{ L mol}^{-1} \quad (10)$$

Here R is the universal gas constant [$\text{J K}^{-1} \text{mol}^{-1}$] and T is the temperature [K].

3. Experimental

3.1 Materials

AN (purity > 99%) was obtained from Wako Chemicals.

3.2 Pressurized differential scanning calorimetry (PDSC)

A Mettler Toledo differential scanning calorimeter (DSC; Mettler Toledo DSCHP27) was used to study the thermal behavior of AN under pressure. A heating furnace of the DSC can be pressurized up to 7 MPa using any gases which is supplied from external compressed gas cylinders or gas supply lines. In this trial, we connected the DSC with an argon gas cylinder using stainless tubes and valves. The experimental setup is shown in Figure 1. In each trial, a sample of approximately 10 mg was placed in an open aluminum pan incorporating a pinhole, following which various pressures were applied (0.1, 0.3, 0.5, 0.7 and 1.1 MPa) in an argon atmosphere, followed by heating from 30 to 350 °C at 5 K min^{-1} with a concurrent 200 mL min^{-1} Ar flow. High pressure was applied during these trials since AN has been found to undergo endothermic evaporation after melting at a pressure of 0.1 MPa and thus either sealing or pressurizing are required to prevent the AN from evaporating. However, too high pressurizing using inert gas dilute evolved gases from AN, and it is difficult to detect the evolved gases under such a condition using MS spectrometer and FT-IR described below. Thus, we investigate thermal behavior of AN under various pressures and determined the sufficient value of pressure.

3.3 PDSC coupled with mass spectroscopy (PDSC-MS)

DSC (Mettler Toledo DSCHP27) coupled with a mass spectrometer (MS; Shimadzu QP-2010) was employed for non-isothermal and isothermal outgassing studies under pressurized conditions (PDSC-MS). The experimental setup is shown in Figure 2. The associated PDSC-MS data were acquired simultaneously to determine the thermal behavior of the AN samples upon heating while evolved gases were analyzed. Approximately 10 mg samples were

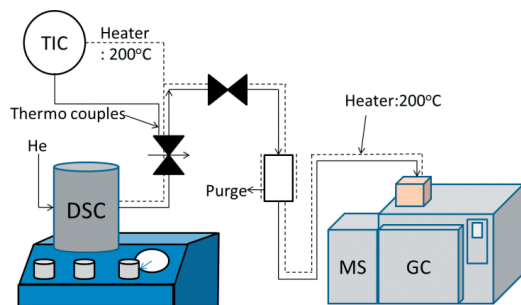


Figure 2 Experimental setup of PDSC-MS.

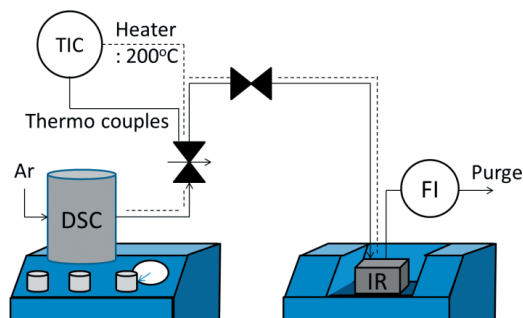


Figure 3 Experimental setup of PDSC-FTIR.

placed in aluminum pans with pinholes and heated from 30 to 350°C at a heating rate of 5 K min⁻¹ at 1.1 MPa under helium with continuous purging at 500 mL min⁻¹ with helium. The evolved gases were transferred to the MS by the helium carrier gas and analyzed. The MS was operated in the electron impact ionization mode with selected ion monitoring for $m/z = 16, 17, 18, 28, 30, 32, 44, 46$ and 63 . As indicated 3.2, optimized pressure is important to detect evolved gases and prevent AN from evaporation. From the results of PDSC, we selected the pressure of 1.1 MPa as one of optimized pressures from the aspects of preventing evaporation and gas detection.

3.4 PDSC coupled with Fourier transform infrared spectroscopy (PDSC-FTIR)

DSC (Mettler Toledo DSC27) coupled with a Fourier transform infrared spectrometer (FT-IR; Shimadzu IR Prestige21) was employed for non-isothermal and isothermal outgassing studies under pressurized conditions. The experimental setup is shown in Figure 3. The PDSC-FTIR data were acquired simultaneously to determine the thermal behavior of the AN samples and to identify the gases evolved upon heating. Samples with masses of approximately 10 mg were placed in aluminum pinhole pans and heated from 30 to 350°C at a heating rate of 5 K min⁻¹ at 1.1 MPa under argon, with a continuous purge of 200 mL min⁻¹ argon. The evolved gases from samples were carried to the gas cell of the FT-IR by the argon carrier gas and their infrared adsorption spectra were acquired. For the same reason indicated 3.3, we selected the pressure of 1.1 MPa.

4. Results and discussion

4.1 Thermal analysis

The DSC profiles obtained from AN under variable pressures are shown in Figure 4. AN is known to evaporate with the appearance of an endothermic peak after melting under a pressure of 0.1 MPa in open conditions^{1),8)}, and to exhibit exothermic reaction under in closed condition or high pressure condition³¹⁾. In the PDSC results, AN exhibits an endothermic reaction above its melting point of 169°C under a pressure of 0.1 MPa. However, the AN also appears to undergo an exothermic reaction above 0.3 MPa and this exothermic process offset the endothermic reaction as the pressure is increased, suggesting that elevated pressures prevent the AN from evaporating.

There are three types of AN decomposition reactions:

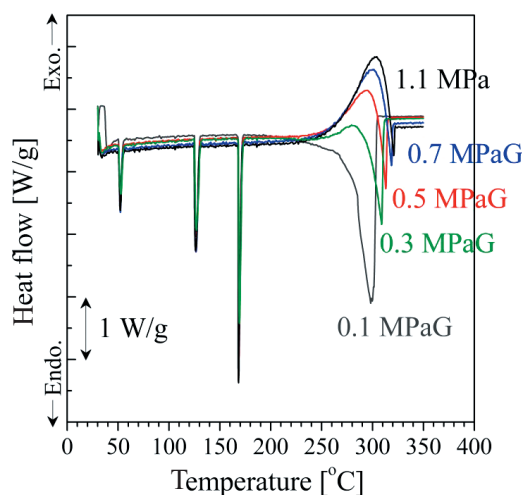


Figure 4 PDSC curves obtained for AN under various initial pressures at a heating rate of 5 K min⁻¹.

condensed phase, gas-liquid two phase and gas phase. Under the 200 mL min⁻¹ argon flow conditions applied in this study, evolved gaseous HNO₃ and NH₃ did not remain in the open sample pan and thus we believe that these PDSC result reflect only the thermal behavior of condensed phase reactions.

4.2 Evolved gas analysis and visual observation

Figures 5 and 6 present the PDSC-MS and PDSC-FTIR profiles obtained for AN at a pressure of 1.1 MPa, indicating that an exothermic reaction occurs above approximately 230°C, exothermic peak top is at approximately 300°C, and an endothermic reaction subsequently starts to take place at above approximately 300°C. In Figure 5, the total ion chromatogram (TIC) plot does not exhibit any increase below the exothermic onset temperature of 230°C, and therefore no gases were evolved from the AN prior to the exothermic reaction. As a result of the 1.1 MPa pressurization, the AN was prevented from evaporating during the endothermic reaction, and thus evolved gases from the exothermic reaction could be analyzed.

In Figure 5, the AN exhibits an exothermic reaction above 230°C, generating gases with fragment masses of 44 and 18. The mass spectra in Figure 5 show the average relative intensities of the ions generated between 230 and 300°C, in which the primary m/z values are 44, 30, 18 and 17. These values are attributed to the production of N₂O ($m/z = 44, 30,$ and $28^{34)}$ and H₂O ($m/z = 18$ and 17^{34}) during the exothermic reaction. In Figure 6, the

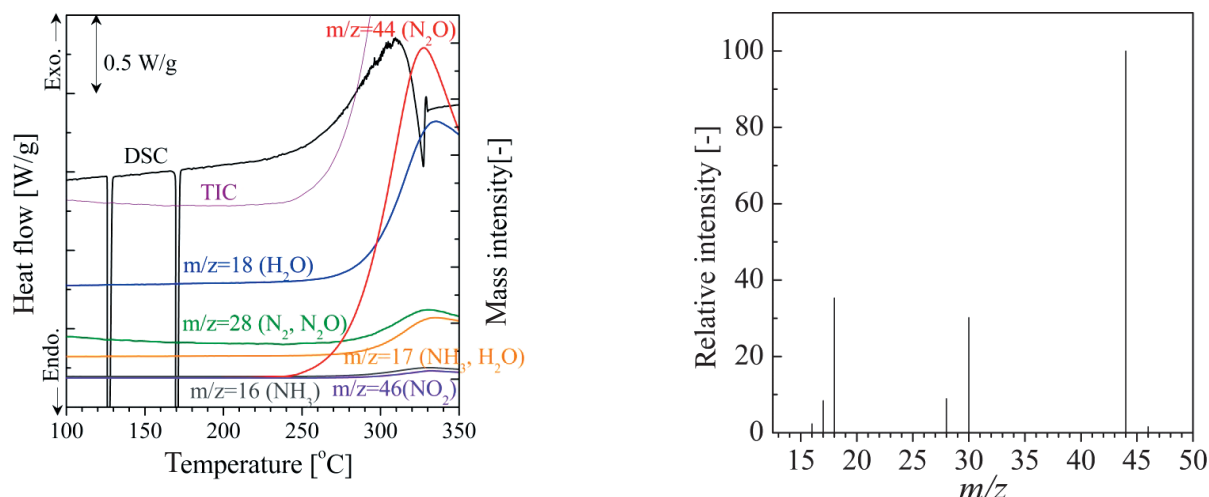


Figure 5 PDSC-MS results for AN under 1.1 MPa at a heating rate of 5 K min⁻¹. The black line indicates PDSC data and colored plots indicate ion intensities. The mass spectrum (right) represents the average ion counts from gases evolved between 230 and 330 °C.

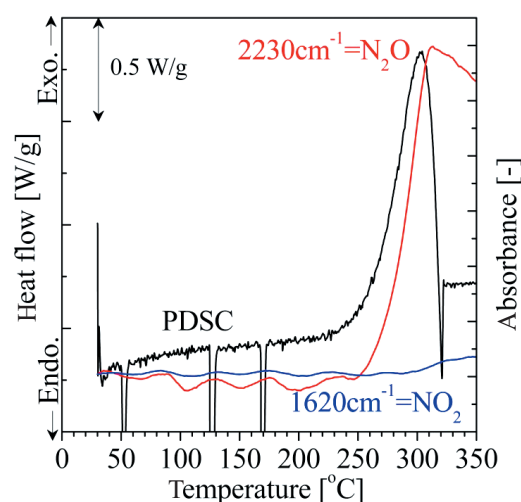


Figure 6 PDSC-FTIR results for AN under 1.1 MPa at a heating rate of 5 K min⁻¹. The black line indicates PDSC data and colored plots indicate absorbance at 2230 cm⁻¹ (red) and 1620 cm⁻¹ (blue).

absorbance at 2230 cm⁻¹, resulting from N₂O³⁴), is seen to increase with the exothermic reaction above 230 °C. Therefore, we conclude that the overall condensed phase decomposition reaction of AN may be written as follows.

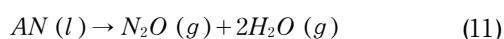
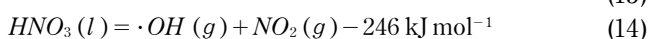
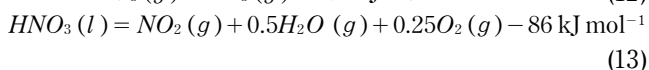
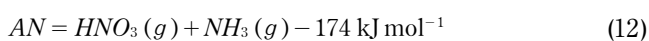
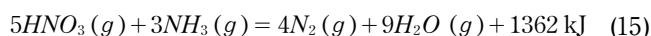


Figure 6 demonstrates that, above 300 °C, the absorbance at 1620 cm⁻¹ resulting from NO₂³⁴) increases as the endothermic reaction proceeds. In Figure 5, ions with *m/z* values of 46, 30, 28, 17 and 16 are observed in conjunction with the endothermic reaction above the same temperature. These ions are attributed to NO₂ (*m/z* = 46 and 30³⁴), N₂ (*m/z* = 28³⁴) and NH₃ (*m/z* = 17 and 16³⁴). It is known that the dissociation of AN to HNO₃ and NH₃ (Equation (12)¹) and the decomposition of HNO₃ (Equations (13) and (14)³⁵) are endothermic.

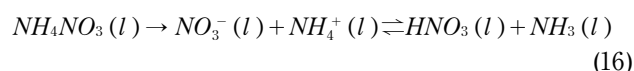


Thus NH₃ will have evolved as in Equation (12) and NO₂ will have been produced as in Equations (13) and (14), while N₂ will have been generated by a radical reaction in the gas phase according to Equation (15). Brower has reported that this radical reaction occurs above 300 °C and proceeds according to this mechanism¹⁴). However, although this mechanism has a high heat of reaction, PDSC measurements in the present study did not show any heat of reaction in the gas phase.



4.3 Modeling of condensed phase decomposition

The concentrations of NO₃⁻ and HNO₃ in the molten AN were calculated based on chemical equilibrium considerations. The equilibrium in molten AN can be represented by the following reaction.



The associated equilibrium constant, *K*_{AN}, was obtained from the following equation.

$$K_{AN} = C_{HNO_3} C_{NH_3} / C_{NO_3^-} C_{NH_4^+} = K_{aNH_4^+} / K_{aHNO_3} \quad (17)$$

Here *K*_a is the acid dissociation constant. The temperature dependence of the equilibrium constant is obtained from Equation (18).

$$\ln K = -\Delta G / RT \quad (18)$$

The following equation is then derived from Equations (17) and (18).

$$\ln K_{AN} = -(\Delta G_{NH_4^+}^0 - \Delta G_{HNO_3}^0) / RT \quad (19)$$

Here ΔG^0 is the standard Gibbs energy change for the acid dissociation; $\Delta G_{NH_4^+}^0$ is 52.8 kJ mol⁻¹, and $\Delta G_{HNO_3}^0$ is 2.5 kJ mol⁻¹³⁵). The concentrations of the various species were obtained from the equations below.

$$C_{HNO_3} = C_{NH_3} = C_{0AN} \sqrt{K_{AN}} \quad (20)$$

$$C_{NO_3^-} = C_{NH_4^+} = C_{0AN} (1 - \sqrt{K_{AN}}) \quad (21)$$

$$C_{0AN} = \rho_{AN} / M_{AN} \quad (22)$$

Here ρ_{AN} is the density of AN (1725 g L^{-1}) and M_{AN} is the molecular weight of AN (80 g mol^{-1}). Substituting Equations (19) and (22) into Equations (20) and (21), we can obtain the concentrations of chemical species, as shown below.

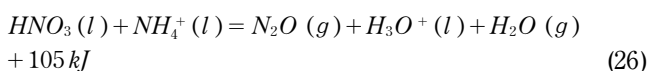
$$C_{HNO_3} = C_{NH_3} = \rho_{AN}/M_{AN} \cdot \exp\left(-1/2(\Delta G_{NH_4^+}^o - \Delta G_{HNO_3}^o)/RT\right) \quad (23)$$

$$C_{NO_3^-} = C_{NH_4^+} = \rho_{AN}/M_{AN} \left[1 - \exp\left(-1/2(\Delta G_{NH_4^+}^o - \Delta G_{HNO_3}^o)/RT\right)\right] \quad (24)$$

We assumed that the condensed phase decomposition of AN proceeded such that liquid HNO_3 oxidized liquid NH_4^+ , and the rate of this reaction may be expressed by Equations (9) and (10). It was also assumed that the concentrations of liquid HNO_3 and NH_4^+ were constant, based on chemical equilibrium, and these assumptions were used to define our AN CPD model. In this model, the heat flow associated with thermal decomposition is obtained from the following equation.

$$q = Q_{AN}/\rho_{AN} \cdot dC_{AN}/dt \quad (25)$$

Here q [$\text{J s}^{-1} \text{ g}^{-1}$] is the heat flow and Q_{AN} is the heat of decomposition (105 kJ mol^{-1}) obtained from Equation (26). As a result, the following equation may be written.



Based on the evolved gas analysis in this study, the main products of the condensed phase decomposition were determined to be N_2O and H_2O . By substituting Equations (9), (10), (23) and (24) into Equation (25), we obtain the calculated heat flow for condensed phase decomposition. Figure 7 presents the heat flow curves obtained from calculations based on the CPD model as well as the experimental results acquired using PDSC. It can be seen that the AN onset temperature and the initial stages of its exotherm were correctly predicted by the CPD model. Thus we conclude that the initial thermal decomposition of AN in the condensed phase proceeds according to the assumptions in the CPD model. However, as the decomposition progresses, the experimental heat flows are evidently lower than the calculated values. The PDSC results shown in Figure 7 suggest an endothermic reaction following the peak exotherm, indicating that some endothermic reactions based on Equations (12) to (14) occurred in the liquid phase AN, offsetting the exothermic reaction predicted by the CPD model.

4.4 Thermal decomposition and combustion mechanism of ammonium nitrate

Figure 8 presents a reaction scheme for the thermal decomposition and combustion of AN, based on the results of this study. In the first step, NO_3^- and NH_4^+ are formed by the dissociation of molten AN above its melting point of 169°C , followed by proton transfer from NH_4^+ to NO_3^- to produce HNO_3 and NH_3 in chemical equilibrium. In the second stage, HNO_3 and NH_3 undergo endothermic vaporization to the gas phase. This vaporization

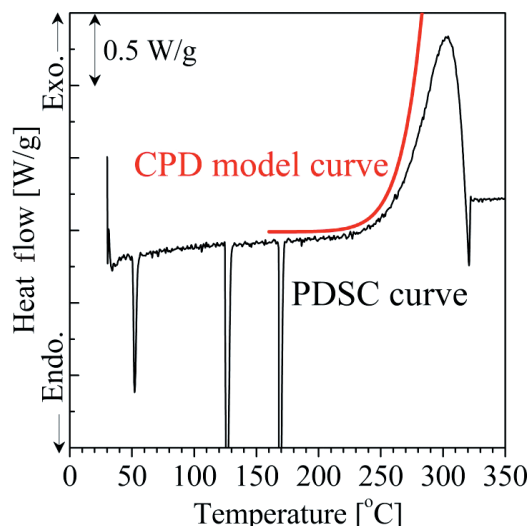


Figure 7 Heat flow curves obtained from AN under 1.1 MPa at 5 K min^{-1} . Theoretical plots are also included, obtained from calculations based on a CPD model using Equation (21).

characterizes the thermal decomposition of AN at 0.1 MPa. As shown in Equation (12), the associated heat of vaporization is significant. Thus, at 0.1 MPa, the AN does not combust but rather decomposes. At elevated pressures, however, the exothermic reaction offsets the endothermic process, since higher pressures prevent the AN from vaporizing and promote the exothermic reaction according to Equation (26). Thus, AN evolves N_2O and H_2O in a condensed phase reaction under high pressure. In the third step, we propose that HNO_3 decomposes to OH radicals and NO_2 above approximately 300°C . Brower has reported that a radical reaction initiated by Equation (5) occurs at above approximately 300°C ¹⁴, while the homolysis of HNO_3 is highly endothermic as shown in Equation (14). Thus, AN exhibits an endothermic reaction in the liquid phase above 300°C . In future, more detailed studies of this endothermic reaction mechanism are required. Finally, evolved gases from the condensed phase combust to produce N_2 , H_2O , O_2 and NO_x in the gas phase^{14, 28}.

5. Conclusions

The PDSC results obtained in this work demonstrated that AN exhibits an exothermic reaction above approximately 230°C at pressures above 0.3 MPa and does not exhibit an endothermic reaction just above its melting point of 169°C . The TIC plot obtained from the PDSC-MS analysis showed that no gases were evolved below 230°C and that evaporation was prevented at 1.1 MPa. There are three types of AN decomposition reactions: condensed phase, gas-liquid and gas phase. The experimental conditions applied in this study, involving an open sample pan under an argon gas flow, did not constrain gases generated by the sample, while evaporation of the AN was inhibited by the application of pressure. Thus, we are confident that the PDSC trials observed only the thermal behavior associated with condensed phase reactions.

PDSC-MS data demonstrated that AN exhibited an exothermic reaction accompanied by the generation of

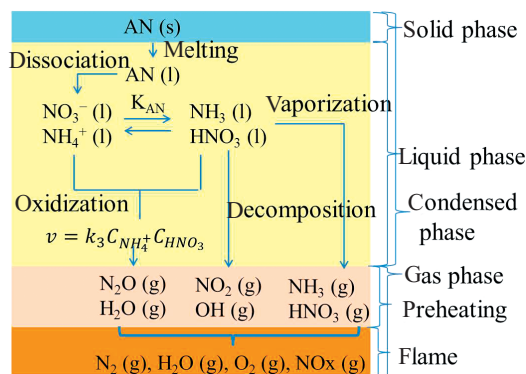


Figure 8 Thermal decomposition and combustion scheme of ammonium nitrate.

gases with fragment masses of 44 and 18, and an endothermic reaction that produced gases having fragment masses of 46, 30, 28, 17 and 16. PDSC-IR data showed that AN underwent an exothermic reaction producing a gas that absorbed at 2230 cm^{-1} (meaning N_2O) and an endothermic reaction accompanied by the evolution of a gas that absorbed at 1620 cm^{-1} (meaning NO_2). Therefore, we conclude that AN evolved N_2O and H_2O during the exothermic reaction above 230°C and generated NO_2 , N_2 and NH_3 during the endothermic reaction. Brower has reported that the radical reaction initiated by $\text{HNO}_3(l) = \cdot\text{OH}(g) + \text{NO}_2(g) - 246\text{ kJ mol}^{-1}$ occurs above 300°C and this reaction proceeds in the gas phase according to equation $5\text{HNO}_3(g) + 3\text{NH}_3(g) = 4\text{N}_2(g) + 9\text{H}_2\text{O}(g) + 1362\text{ kJ}$. Thus, we believe that N_2 is evolved from a gas phase radical reaction.

A CPD model was proposed in which the condensed phase decomposition of AN proceeds in such a manner that liquid HNO_3 oxidizes liquid NH_4^+ , as summarized by $\text{HNO}_3(l) + \text{NH}_4^+(l) = \text{N}_2\text{O}(g) + \text{H}_3\text{O}^+(l) + \text{H}_2\text{O}(g) + 105\text{ kJ}$. At chemical equilibrium, where ΔG_{HNO_3} and $\Delta G_{\text{NH}_4^+}$ are constant, the rate of this reaction is expressed by equations $-dC_{\text{AN}}/dt = 10^{9.4} \exp(-126000/RT) C_{\text{AN}}^2 \sqrt{K_{\text{AN}}} (1 - \sqrt{K_{\text{AN}}})$. A simulated heat flow curve generated by this CPD model predicts an exothermic reaction above approximately 230°C and is in good agreement with the initial exothermic behavior of AN as observed in the PDSC data acquired at 1.1 MPa. Therefore, we conclude that the initial condensed phase decomposition of AN proceeds according to the mechanism proposed in the CPD model.

The reaction scheme for the thermal decomposition and combustion of AN is summarized in Figure 8. In this scheme, the melting of AN is followed by two endothermic reactions, the vaporization of NH_3 and HNO_3 and the decomposition of HNO_3 , along with the exothermic oxidation of NH_4^+ by HNO_3 . These reactions proceed in parallel in the liquid phase.

References

- 1) C. Oommen and S. R. Jain, *J. Hazard. Mater.*, A67, 253–181 (1999).
- 2) J. C. Oxley, J. L. Smith, E. Rogers, and M. Yu, *Thermochimica Acta.*, 384, 23–45 (2002).
- 3) G. Marlair and M. Kordek, *J. Hazard. Mater.*, A123, 13–28 (2005).

- 4) Chemical Safety Board. "Preliminary Findings of the U.S. Chemical Safety Board from its Investigation of the West Fertilizer Explosion and Fire", <http://www.csb.gov/assets/1/19/West_Preliminary_Findings.pdf> (accessed : 15-January-2013) (online).
- 5) N. Dechy, T. Bourdeaux, A. Ayrault, M. Kordek, and J. L. Coze, *J. Hazard. Mater.*, 111, 131–138 (2004).
- 6) V. P. Sinditskii, V. Y. Egorshv, A. Y. Levshenkov, and V. V. Serushkin, *Propellants Explos. Pyrotech.*, 30, 269–280 (2005).
- 7) V. P. Sinditskii, V. Y. Egorshv, V. V. Serushkin, and S. A. Filatov, *Combust Expl Shock Waves.*, 48, 81–99 (2012).
- 8) K. Kajiyama, Y. Izato, and A. Miyake, *J. Therm. Anal. Calorim.*, 113, 1475–1480 (2013).
- 9) Y. Izato, A. Miyake, and S. Date, *Prop. Explos. Pyrotechnics*, 38, 129–135 (2013).
- 10) A. Miyake and Y. Izato, *Intl. J. Energetic Materials and Chemical Propulsion*, 9, 523–531 (2011).
- 11) Y. Izato, H. Echigoya, and A. Miyake, *Sci. Tech. Energetic Materials*, 70, 101–104 (2009).
- 12) Y. Izato, K. Kajiyama, and A. Miyake, *Sci. Tech. Energetic Materials*, 75, 128–133 (2014).
- 13) J. C. Oxley, J. L. Smith, and W. Wang, *J. Phys. Chem.*, 98, 3901–3907 (1994).
- 14) K. R. Brower, J. C. Oxley, and M. Tewari, *J. Phys. Chem.*, 89, 4029–4033 (1989).
- 15) G. B. Manelis, G. M. Nazin, Y. I. Rubtsov, and V. A. Strunin, Taylor & Francis, 175–187 (2003).
- 16) Y. Wada, M. Arai, *Sci. Tech. Energetic Materials*, 71, 39–43 (2010).
- 17) Y. Miyata and K. Hasue, *J. Energ. Mater.*, 29, 344–359 (2011).
- 18) M. Pandey, S. Jha, R. Kumar, S. Mishra, and R. R. Jha, *J. Therm. Anal. Calorim.*, 107, 135–140 (2012).
- 19) A. G. Keenan, K. Notz, and N. B. Franco, *J. Am. Chem. Soc.* 3168–3171 (1969).
- 20) J. H. Macneil, H. Zhang, P. Berseth, and W. C. Troglor, *J. Am. Chem. Soc.* 119, 9738–9744 (1997).
- 21) X. R. Li and H. Koseki, *Process Safety and Environmental Protection*, 83, B1, 31–37 (2005).
- 22) J. Sun, Z. Sun, Q. Wang, H. Ding, T. Wang and C. Jiang, *J. Hazard. Mater.*, B127, 204–210 (2005).
- 23) J. C. Oxley, J. L. Smith, S. Naik, and J. Moran, *J. Energe. Mater.*, 27, 17–39 (2009).
- 24) V. A. Koroban, *Propellants Explos. Pyrotech.*, 19, 307–310 (1994).
- 25) D. G. Patil, S. R. Jain, and T. B. Brill, *Propellants Explos. Pyrotech.*, 17, 99–105 (1992).
- 26) A. Mirvakili, F. Samimi, and A. Jahanmiri, *J. Ind. Eng. Chem.*, 20, 2452–2462 (2014).
- 27) S. A. Skarlis, A. Nicolle, D. Berthout, C. Dujardin, and P. Granger, *Thermochimica Acta.*, 584, 58–66 (2014).
- 28) S. Cagnina, P. Rotureau, G. Fayet, and C. Adamo, *Phys. Chem. Chem. Phys.*, 15, 10849–10859 (2013).
- 29) Y. Wada, K. Hori, and M. Arai, *Sci. Tech. Energetic Materials*, 71, 83–87 (2010).
- 30) K. Hasue, R. Miura, and K. Yoshitake, *Sci. Tech. Energetic Materials*, 74, 113–117 (2013).
- 31) K. Fujisato, H. Habu, A. Miyake, and K. Hori, *Sci. Tech. Energetic Materials*, 75, 28–36 (2014).
- 32) K. Ikeda, Y. Shiraishi, and S. Date, *Sci. Tech. Energetic Materials*, 75, 59–63 (2014).
- 33) K. Ikeda, A. Doi, and S. Date, *Sci. Tech. Energetic Materials*, 75, 83–85 (2014).
- 34) NIST chemistry web book. <http://webbook.nist.gov/chemistry/> accessed 3 September 2014.
- 35) D. D. Wagman, W. H. Evans, V. B. Parker, R. H. Schumm, I. Halow, S. M. Bailey, K. L. Churney, and R. L. Nuttall, *The NBS tables of chemical thermodynamic properties. J. Phys. Chem. Ref. Data.* ; 11supl.2; 67–72 1982.